Research Article

Do Tra Huong*, Nguyen Van Tu, Ha Xuan Linh, Nguyen Thi Hien Lan, Nguyen Quoc Dung, Chu Manh Nhuong, Nguyen Khanh Long, Truong Xuan Vuong, and Thi Kim Ngan Tran*

Applying nanocarbon prepared from coal as an anode in lithium-ion batteries

https://doi.org/10.1515/gps-2024-0151
received July 04, 2024; accepted October 08, 2024

Abstract: Carbon materials is a commonly used electrode material because of its low cost, good conductivity, and structure that allows lithium ions to intercalate between layers in the carbon network. In this article, carbon nanomaterials (CP) have been successfully manufactured from Vietnamese coal. CP is a two-dimensional, leaf-shaped nanomaterial with a specific surface area of 16.7799 $m^2 \cdot g^{-1}$. In the symmetric supercapacitor system, the CP electrode has a high specific capacitance rate of 275 $F \cdot g^{-1}$ with a current density of 0.1 $A \cdot g^{-1}$, an energy density of 6.4 $W\,h \cdot kg^{-1}\,g^{-1}$, and outstanding cyclic stability with capacitance retention of 83.1% after 1,000 cyclic voltammetry curves in 6 M potassium hydroxide electrolyte solution. When using the CP electrode as the anode in a lithium-ion battery (LIB) with a solution of lithium hexafluorophosphate, dimethyl carbonate, ethylene carbonate, and diethyl carbonate at 1:1:1 (v/v/v) ratio and concentration of 1.0 M. LIB has a specific capacity of 336.0 mA $h \cdot g^{-1}$ at *C*/10 and 425.5 mA $h \cdot g^{-1}$ at C/20 (C = 372 mA $h \cdot g^{-1}$). When discharged, the CP electrode operates stably and can integrate Li ions well. Therefore, excellent electrochemical performance verifies the potential of nanocarbon materials production from coal on a large scale for high-performance anode in LIBs.

*** Corresponding author: Do Tra Huong,** Chemistry Faculty, Thai Nguyen University of Education, Thai Nguyen, 250000, Vietnam, e-mail: huongdt.chem@tnue.edu.vn
*** Corresponding author: Thi Kim Ngan Tran,** Institute of Applied Technology and Sustainable Development, Nguyen Tat Thanh University, Ho Chi Minh City, 700000, Vietnam, e-mail: nganttk@ntt.edu.vn
Nguyen Van Tu: Institute of Materials Chemistry – Institute of Military Science and Technology, Hanoi 143315, Vietnam
Ha Xuan Linh: International School, Thai Nguyen University, Thai Nguyen, 250000, Vietnam
Nguyen Thi Hien Lan, Nguyen Quoc Dung, Chu Manh Nhuong, Nguyen Khanh Long: Chemistry Faculty, Thai Nguyen University of Education, Thai Nguyen, 250000, Vietnam
Truong Xuan Vuong: University of Science – Thai Nguyen University, Thai Nguyen, 250000, Vietnam

Keywords: porous carbon, coal, hydrothermally, supercapacitor, specific capacity

1 Introduction

Energy crisis is a global concern due to its profound impact on various sectors, including industry, agriculture, tourism, and human life. Today, numerous technological fields such as transportation, portable electronics, medical equipment, electric tools, and electricity storage from renewable sources (e.g., wind, solar, and tidal) have been significantly advanced. This development has led to an increasing demand for rechargeable batteries, including those being used for laptops, bicycles, and electric cars. Therefore, extended battery recharge time is one of the desirable properties to users. Therefore, researchers are constantly seeking solutions to improve the energy storage capacity of batteries, thus increasing the battery life. Lithium-ion rechargeable batteries (Li-ion) are currently considered an optimal energy storage solution as the batteries have high energy density and a relatively simple reaction mechanism. Currently, popular cathode electrode materials are $LiCoO_2$ with a layered structure and $LiMn_2O_4$ with a three-dimensional spinel structure. Besides, graphite is also used as an anode material for commercial Li-ion batteries (LIBs) because of its lifelong cycle and low cost. However, the low theoretical specific capacity (only about 372 mA $h \cdot g^{-1}$) of graphite remains a major limitation for its application in high-energy storage devices, such as electric cars and bicycles. Therefore, developing a new anode material that can overcome this limitation is an urgent demand for scientists worldwide.

Carbon nanotubes, graphene, and carbon-based materials are of interest to many researchers [1,2]. However, to meet the increasing demand, it is necessary to find abundant and cheap reserves. Coal is one of the world's most abundant fossil energy sources. Coal consists of heterogeneous molecules forming a three-dimensional cross-linked structure. The organic macromolecules of coal are made up of a combination of aromatic/hydroaromatic nuclei and

aliphatic nuclei. These nuclei are connected by ether bonds and short aliphatic bonds [3]. Furthermore, a high degree of charring of coal is found to be associated with a high content of fragrant compounds and carbon, as seen in anthracite coal, lignite, and bitumen, which has a carbon content of more than 90%, 60–75%, and 75–90%, respectively [4]. Lower-rank coals, such as lignite and sub-bituminous coal, are rich in oxygen-containing functional groups and various heteroatoms. These chemical characteristics contribute to their diverse functional activities. Some key features, such as oxygen-containing groups (phenolic acids, carboxylic acids, aliphatic ethers, cross-linked aryl-O, quinone analogs, and furan analogs), are important for the thermal stability and potential use in polymer production. The presence of these diverse functional groups and heteroatoms imparts lower-rank coals with a wide range of potential applications such as catalysis, adsorption, electrochemical applications, and metal recovery [5]. Nanocarbon materials derived from coal hold show promise due to their eco-friendly nature, ease of synthesis, and cost-effectiveness. Their synthesis often involves controlled pyrolysis or other methods that convert coal into nanoscale carbon structures, offering a sustainable alternative to traditional carbon materials. Numerous studies have focused on synthesizing carbon materials from coal. Examples include the production of three-dimensional (3D) porous graphene from coal tar [6], porous carbon from coal tar [7], graphene quantum dots from bituminous coal [8], porous graphene from anthracite coal [9], porous carbon from coal [10,11], potassium hydroxide (KOH)-activated carbon nanocomposites from coal [12], and a two-dimensional (2D) structure from coal with oxygen-rich porous carbon nanosheets (OPCN-700) [13].

Carbon materials derived from coal used to store energy, such as batteries and supercapacitors, have been widely studied. For example, porous graphene with a large specific surface area (640 $m^2 \cdot g^{-1}$) and micro-meso pores was synthesized from anthracite coal to produce a high-performance electrode material for lithium-ion batteries (LIBs). [9]. The battery maintained 98% efficiency after 110 charge–discharge cycles and can have a specific 770 mA $h \cdot g^{-1}$ capacity at $C/10$. A possible explanation for this is that the structure of graphene increased the diffusion and transport of Li^+ ions. Another study by Li et al. fabricated spherical porous carbon nanomaterials with uniform morphology from coal as anode electrodes in LIBs with 1,188.9 mA $h \cdot g^{-1}$. The Li^+ ion transport distance is reduced by the large surface area of the material, thereby improving capacity and charge cycle stability [11]. Oxygen-rich porous carbon nanosheets (OPCN-700) with a 2D structure, derived from coal, were synthesized by Che et al. [13]. These nanosheets have a large surface area of 2.388 $m^2 \cdot g^{-1}$, a high oxygen content of 24.4%, and good wetting ability. In addition, the rich 2D micro-pores and nanosheet structure of OPCN-700 help to effectively store and transport electrolyte ions. Therefore, when the supercapacitor operates, it has a specific capacitance of 382 $F \cdot g^{-1}$ at J = 0.5 $A \cdot g^{-1}$.

To fabricate carbon nanomaterials from coal, researchers often activate the coal using potassium hydroxide KOH [14], K_2CO_3 [15], or through hydrothermal carbonization (HTC) followed by steam activation [16], or $ZnCl_2$ [17]. During the carbon fabrication process from coal, $ZnCl_2$ plays a role in creating numerous voids within the material, thereby increasing its porosity. Additionally, $ZnCl_2$ activation reduces the oxygen content of the products and further enhances their electrical conductivity [17]. However, to date, there have been very few studies on the fabrication of activated carbon using $ZnCl_2$, and no published works have combined the hydrothermal method with $ZnCl_2$ as an activating agent in the process of synthesizing carbon nanomaterials from coal.

Vietnam is one of three countries that possesses the most significant amount of exploitable coal in Southeast Asia, along with Indonesia (34.87 billion tons) and Thailand (1.06 billion tons). According to the Vietnam Coal and Mineral Corporation, coal reserves in Vietnam are about 50 billion tons, of which exploitable reserves are 3.7 billion tons distributed mainly in the Northeast coal basin. In the Song Hong coal basin, coal mines in other provinces are about 400 million tons. However, no author in the country or around the world has researched the production of carbon nanomaterials from coal sources by activating $ZnCl_2$ combined with a hydrothermal method to make an anode in LIBs. Therefore, in this article, we present the results of (1) manufacturing porous carbon materials using the hydrothermal method combined with $ZnCl_2$ activation from coal sourced from the Phan Me Coal Mine (Phu Luong, Thai Nguyen, Vietnam), and (2) investigating the lithium-ion storage capacity of these carbon nanomaterials when used as anode materials in lithium-ion batteries (LIBs). The material's characteristics, morphology, composition, structure, and specific surface area of the material were studied. The electrochemical properties of the electrode and Li-ion battery were examined by using scanning multi-cyclic voltammograms (CV), constant current charging, and total impedance.

2 Materials and methods

2.1 Chemical

Zinc chloride (Merk, CAS 7646-85-7|108816) and KOH pellets were procured from Sinopharm Chemical Reagent Co.,

Ltd. Lithium hexafluorophosphate ($LiPF_6$), diethyl carbonate (DEC) ($C_5H_{10}O_3$, 99%), and dimethyl carbonate (DMC) ($C_3H_6O_3$, ≥99%) was obtained from Suzhou Duoduo Chemical Material Co., Ltd. The solvent *N*-methylpyrrolidine was sourced from A1 Vietnam Company, a US supplier. Polyvinylidene fluoride (PVDF) polymer adhesive was acquired from Shandong Hengyi New Material Technology Co., Ltd., China.

2.2 Fabrication of nanocarbon

Coal was crushed and sieved into powder with particle size of less than 0.5 mm and was denoted as CD. CD was then mixed with solid $ZnCl_2$ in different mass ratios (e.g., 4:1, 2:1, 3:1, and 1:1). The mixture was ground in an agate mortar and transferred into a 100 mL Teflon with lid. The paste was made with the help of distilled water and stirred continuously for 1 h. Then, the mixture was transferred to an autoclave flask and heated at 200°C for 3 h. The samples were heated at 900°C for 6 h, removed and neutralized several times with 0.5 M HCl solution; the solution was then centrifuged for 15 min at 4,000 rpm of speed. The solid sample was collected, and the solution was adjusted to pH 7 using distilled water. The sample was then heated at 110°C until its mass remained constant. The resulting material, referred to as CP (Carbon Porous), was subsequently placed in a desiccator.

2.3 Select the optimal CD:$ZnCl_2$ ratio

The scanning electron microscope (SEM) results in Figure 1 show that the fabricated material samples have a mass ratio of CD:$ZnCl_2$ = 1:1, 2:1, 3:1, and 4:1. This shows that the samples are all nanometers in size. However, the sample with a CD:$ZnCl_2$ ratio of 3:1 has a porous surface and a more uniform particle size. This is consistent with the BET surface area measurements, which show that the samples with mass ratios of CD:$ZnCl_2$ are 1:1, 2:1, 3:1, and 4:1 have corresponding surface areas of 13.4585, 15.6905, 16.7799, and 10.202 $m^2 \cdot g^{-1}$, respectively. The samples with ratios of them are 2:1 and 3:1 exhibit the largest surface areas with negligible differences between them. However, from an economic perspective, the sample with a ratio of 3:1 should be preferred. Therefore, we select the mass ratio CD:$ZnCl_2$ of 3:1 as the optimal ratio to prepare CP porous carbon material from CD by the hydrothermal method. The schematic diagram of the fabrication of CP porous carbon nanomaterials is shown in Figure 2.

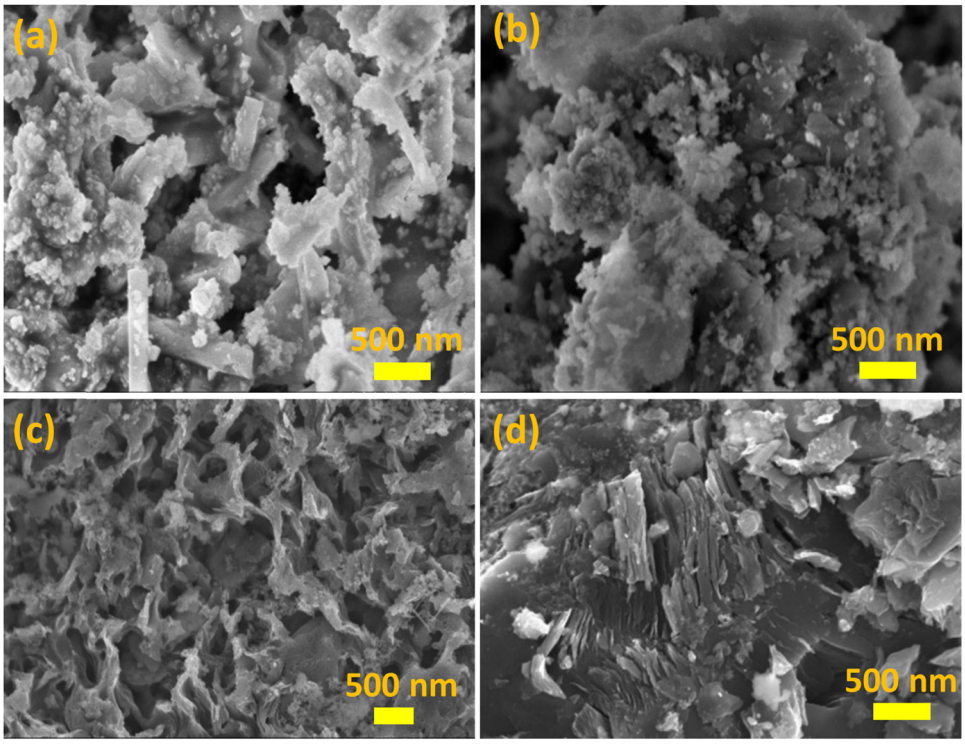

Figure 1: SEM image of the material CD: (a) CD:$ZnCl_2$ = 1:1, (b) CD:$ZnCl_2$ = 2:1, (c) CD: $ZnCl_2$ = 3: 1, and (d) CD:$ZnCl_2$ = 4:1.

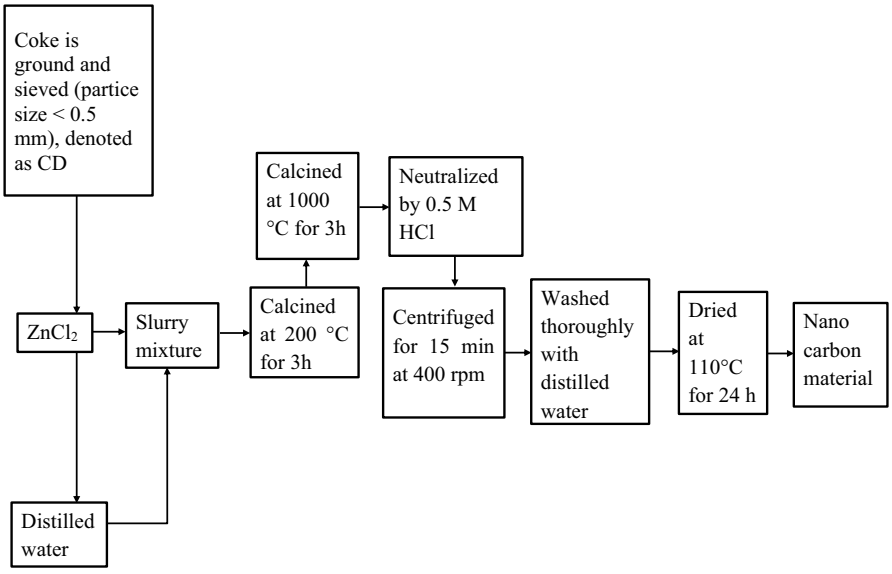

Figure 2: Scheme of CP fabrication.

2.4 Fabrication of CP electrodes

The CP electrode is made from porous carbon material according to Figure 3.

2.5 Manufacturing LIBs

The anode in the Li-ion battery was fabricated as follows: CP carbon nanopowder, conductive additive (graphite:-carbon nanotube), and PVDF binder were mixed in an appropriate amount of polyvinylidene polymer solvent in a mass ratio of 7:1:1:1. Then, the mixture was cast onto nickel foil and dried under vacuum at 80°C for 5 h. After cutting, an electrode plate with a diameter of 14 mm was obtained. The mass loading of CP material is about 0.35 g·cm^{-2}.

The battery was fabricated in a coin cell form (with a diameter of 20 mm and a height of 3.2 mm), the cathode was a circular LFP electrode with a diameter of 14 mm, the anode was a circular CP electrode with a diameter of 14 mm, and the separator was a polyethylene membrane with a diameter of 16 mm. The electrolyte was a solution of 1 M $LiPF_6$ in a mixture of ethyl methyl carbonate, ethylene carbonate (EC), and DMC in a ratio of 1:1:1 by volume.

The batteries were fabricated in the following order: battery shell > anode > diaphragm layer > cathode > gasket > gasket > battery cover using a 100 Pcs CR2032 Case battery press – MSK-110.

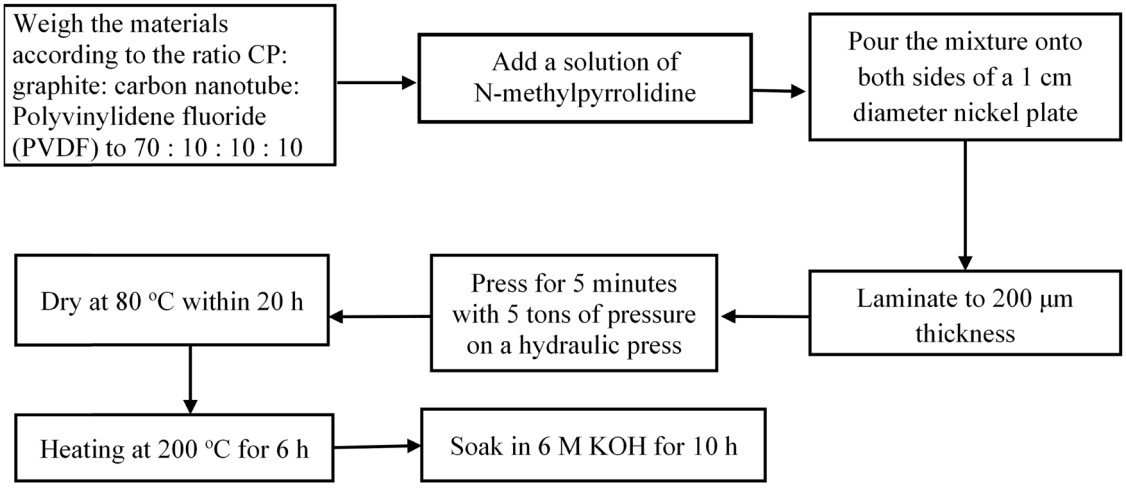

Figure 3: CP electrode fabrication diagram.

The battery assembly took place in a highly controlled environment within an isolated cabinet filled with pure argon gas at the Institute of Chemistry, Military Institute of Science and Technology. This controlled environment ensures the integrity and reliability of the manufacturing process. The assembled battery was then kept stable for 24 h.

2.6 Physicochemical characteristics of CD and CP

The physical properties and surface characteristics of CD and CP were investigated using a range of advanced equipment. SEM and transmission electron microscope (TEM) measurements were performed using MS-7001F and a JEM-2001F (Jeol-Japan), respectively. The EDX method, which determines sample composition, was performed on an MS-7001F device (Jeol, Tokyo, Japan). The X-ray diffraction (XRD) method was performed on a D8 ADVANCE; Bruker, Bremen, Germany. The FT-IR infrared spectrum is measured on a Jasco 6300, Japan. The sample surface area was measured on a Tristar 3000 micromeritics. The thermal analysis method was measured on a Labsys TG/DSC 1600, TMA-SETARAM machine, differential thermal gravimetric analyzer (TG-DT-8121, France). The Raman spectrum of the sample was conducted by Micro-Raman LAB RAM, 1B Jobin, Yvon (France).

2.7 Electrochemical measurement

Measurements of electrochemical properties to study the ability of CP electrodes to store and release energy were conducted on the AutoLab PGSTAT100 system, the Netherlands. Electrochemical measurements in a tri-electrode system with the working electrode made from CP material. The reference electrode is saturated calomel, and the counter electrode is Pt. The measuring solution is 6 M KOH. The two-electrode system was set up as follows: prepare two identical CP electrodes; one is the working electrode, and the other is connected to the reference and the counter electrodes. The two-electrode system was measured in a 6 M KOH solution.

The electrochemical properties of the CP anode electrode in LIBs were measured on BaSyTec CTS – LAB (Battery Test System) equipment.

3 Results

3.1 Physicochemical characteristics of CD and CP

Results of thermal analysis of CP material are shown in Figure 4a.

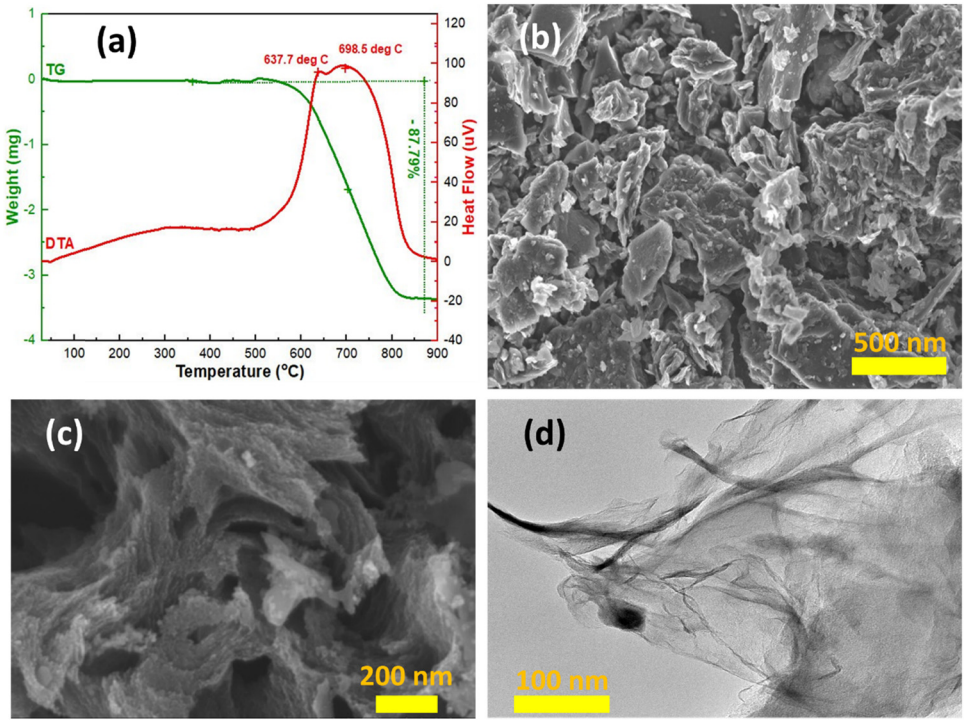

Figure 4: (a) TG and DTA measurement results of CP, (b) SEM image of CD material, (c) SEM image of CP, and (d) TEM image of CP.

The DTA line in Figure 4a shows two exothermic effects at 637.7°C and 698.5°C. The TG curve shows a mass loss in the temperature range of 500°C to 820°C, with a total mass loss of 87.79%, which corresponds to the heat released during the combustion of organic matter and volatile substances in CP [18]. The sample mass remains unchanged from 820°C.

The SEM and TEM images reveal a porous structure, smaller in size than CD (Figure 3b), with a structural hierarchy corresponding to macropores, mesopores, and micropores, and PC is a 2D layered nanomaterial (Figure 4c and d). The EDX analysis results (Figure 5a) further confirm the uniqueness of CP, of which the main components are C (88.74% in mass), O (6.3% in mass), and trace and insignificant amounts of Al, Si, S, Fe, and Zn. In comparison to Do et al. [19], which employed the Hummer method to synthesize carbon nanomaterials with a carbon content of 80.88% by weight from coal, the CP synthesized from a hydrothermal method in this study has a higher carbon content.

The XRD pattern (Figure 5b), which was prepared on a standard card (PCPDF No: 89-8487), shows that CP has a diffraction peak (002) at an angle of 2θ = 24.5°, corresponding to amorphous carbon, and at an angle of 2θ = 43°, a diffraction peak (001), corresponding to the graphite structure. This indicates that the sample has an amorphous carbon and graphite structure [18], which is of great importance in our study.

Raman spectroscopy was performed to elucidate the structural properties of the graphene material. Figure 5c and d show that both CD and CP materials exhibit extended in-plane vibrations of C═C at the G-band (1,592 cm^{-1}) [20]; due to graphite oxidation, the wavenumber is significantly higher (1,570 cm^{-1}). The D-band (1,349 cm^{-1}) indicates the formation of defects at sp^2 hybridized carbon edges [21]. Additionally, the 2D band (2,945 cm^{-1}) shows a very small peak for CP, attributed to the disruption of stacking order layers [22]. The CD is activated into CP by a hydrothermal method combined with $ZnCl_2$ activation, which peels off the graphite plane and then oxidizes it completely into graphene oxide. This shows that the CP material will provide more electrochemical reaction sites and improve the reaction rate occurring on the material surface, thus increasing the Li-ion battery's storage capacity and specific capacity. The 2D-band CD peak (2,945 cm^{-1}) has a sharp peak and a high and sharp base, showing the presence of more edges and defects in the CD microstructure. This is consistent with

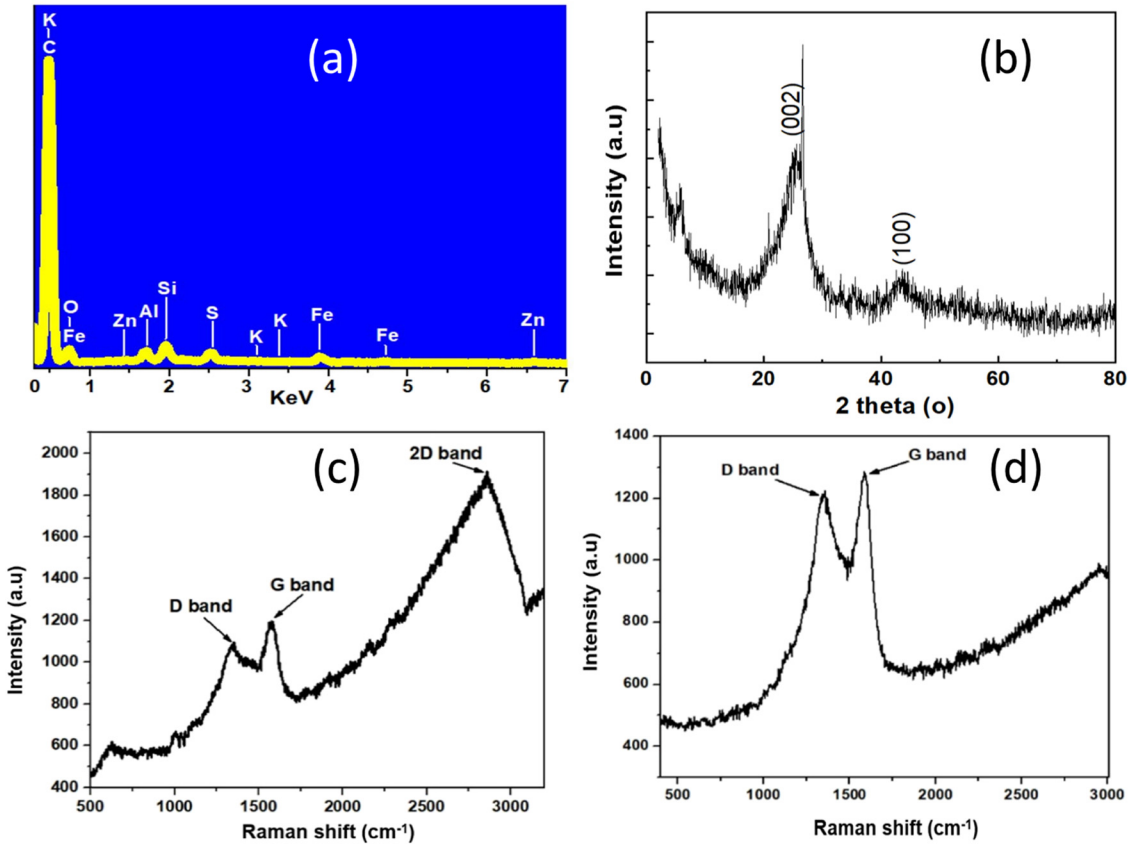

Figure 5: (a) EDX spectrum of CP, (b) XRD pattern of CP, (c) CD Raman spectrum, and (d) CP Raman spectrum.

the results of CDCP carbon material made from coal by the Hummer method [19].

The FT-IR spectrum results of CP in Figure 6a provide practical insights. The weak spectral pattern at frequency 1,710.93 cm^{-1} is the vibration of the C═C group, a key component in our material. The intense spectral pattern at the frequency of 1,665.60 cm^{-1} is the valence vibration of the carbonyl group C═O and the amide group [23], indicating the potential for diverse applications. The absorption of the CH_3 group at spectral fringes of 1,385.91 and 1,303.94 cm^{-1} [24] further enhances the practicality of our findings. The absorption bands at 1,000–1,300 cm^{-1} are related to C–O valence vibrations in acid, alcohol, phenol, ether, and/or ester groups [25], a wide range of potential applications. The absorption bands at 750–600 cm^{-1} are assigned to the deformation vibrations of the out-of-plane bending OH group [24], another aspect that could lead to practical applications.

Figure 6b shows that the CP nitrogen adsorption and desorption isotherms follow type IV isotherm, hysteresis loop H4, with particle size from microcapillary to medium capillary [26,27]. According to the classification according to the IUPAC classification system (USA), the pore diameters can have variable diameters (d): tiny pores (d < 2.0 nm), medium pores (2.0 nm < d < 50 nm), and macropores (d > 50 nm) [28]. As shown in Figure 5b, the specific surface area of CP is calculated to be 16.7799 $m^2 \cdot g^{-1}$, and the inset in Figure 6b shows the pore width is 3.88 nm that confirms the medium pores of material (Figure 6b). Additionally, the CP material has a specific density of 0.5 $g \cdot cm^{-3}$. This shows that CP material is light and porous.

The research results on surface characteristics, structure, composition, surface functional groups, and specific surface area show that CP materials have been manufactured from CD.

3.2 Evaluate the ability of CP to store and release energy

3.2.1 Multi-cyclic voltammograms

The electrochemical properties of CP acted as a supercapacitor were measured in a 6 M KOH electrolyte solution, a three-electrode system, at room temperature. The CV curves were used to evaluate the energy storage and release the capacity of the CP electrode quickly. The CP electrode was scanned with a scan rate varying from 30 to 100 $mV \cdot s^{-1}$. After the CP electrode operated stably, multi-cycle scanning was continued up to 1,000 cycles scan rate of 100 $mV \cdot s^{-1}$, the potential sweep range from −0.7 to 0.5 V/SCE. The cyclic voltammograms of the CP electrode at different scan rates are shown in Figure 7.

Figure 7a illustrates that the CV curves at different scan rates exhibit an almost rectangular shape with no prominent redox peaks. The CV curve at a scan rate of 100 $mV \cdot s^{-1}$ is more typical compared to the curve at 30 $mV \cdot s^{-1}$, indicating a larger specific capacitance. This also demonstrates effective energy release in the electric double layer, with the electrode performing well as the scanning speed increases.

As shown in Figure 7b, following the activation process, the number of charging and discharging cycles directly influences the positive and negative current values of the CP. Specifically, these values gradually decrease, indicating a reduction in the energy storage capacity of the CP during the

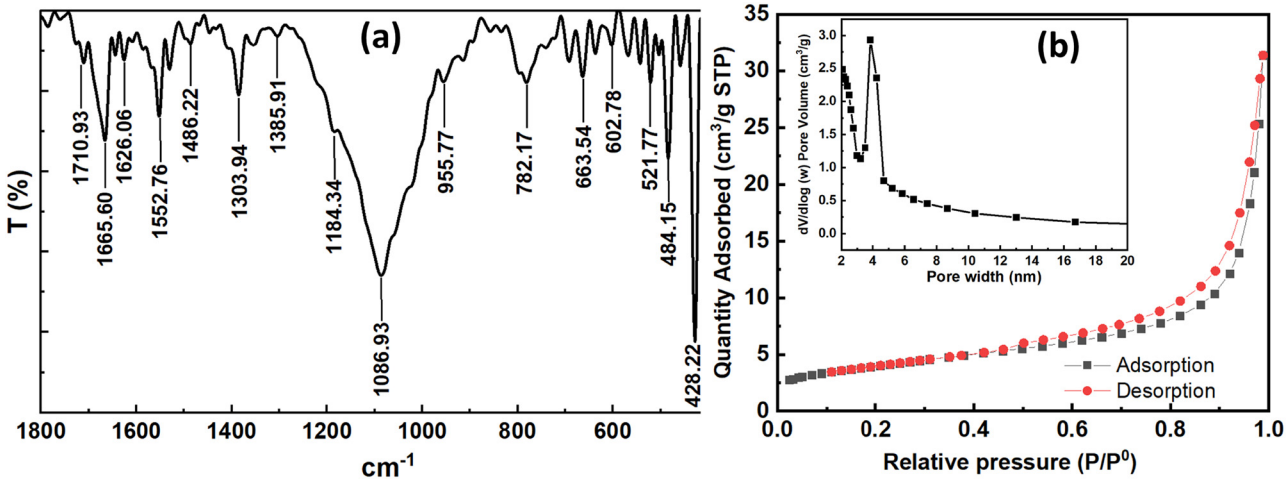

Figure 6: (a) FT-IR spectrum of CP and (b) nitrogen adsorption and desorption isotherms of CP.

charging process. This trend is a direct result of the number of cycles. To quantify this, the specific capacitance of the CP is determined using the CV method as outlined below [19]:

$$C = \frac{\int_{E_i}^{E_f}(E)\mathrm{d}E}{2mv(E_f - E_i)} \quad (1)$$

where m is the mass of material (g), potential scan rate ($mV{\cdot}s^{-1}$), and C is the specific capacitance ($F{\cdot}g^{-1}$).

The results show that in the first cycle, the specific capacitance of the CP electrode is 7.193 $F{\cdot}g^{-1}$; at 500 CV, the specific capacitance is equal to 6.652 $F{\cdot}g^{-1}$, and at 1,000 CV, the specific capacitance is equal to 5.848 $F{\cdot}g^{-1}$. The results show that after 500 CV, the specific capacitance of CP decreases by 92.24%; after 1,000 CV, it decreases by 81.3% compared to the initial specific capacitance.

3.2.2 Charge and discharge

CP was discharged and charged by applying a constant current (GCD) with a current density ranging from 0.1 to 0.5 $A{\cdot}g^{-1}$ for 1,000 s, with the voltage varying between −0.20 V and 0.1 V. The results are shown in Figure 6c. The discharge and charging paths are triangular and symmetrical. No voltage drop was observed at high current densities, suggesting that the material can store energy on the electrode through physical adsorption to form electrical double layers.

The specific capacitance of the electrode, a crucial parameter in energy storage, can be reliably calculated using the discharge–charge method [19].

$$C = \frac{4J\Delta t}{\Delta V m} \quad (2)$$

where J is the current density ($A{\cdot}g^{-1}$), Δt is the launch time (s), and ΔV is the working voltage (V).

The results of calculating the specific capacitance using the charge-discharge method show that the highest specific capacitance of CP is 275 $F{\cdot}g^{-1}$ at J = 0.1 $A{\cdot}g^{-1}$, and the smallest is 123 $F{\cdot}g^{-1}$ at J = 0.5 $A{\cdot}g^{-1}$.

The results in Table 1 show that CP's specific capacitance C ($F{\cdot}g^{-1}$) is relatively high compared to other carbon electrodes derived from coal. Also, from the results of

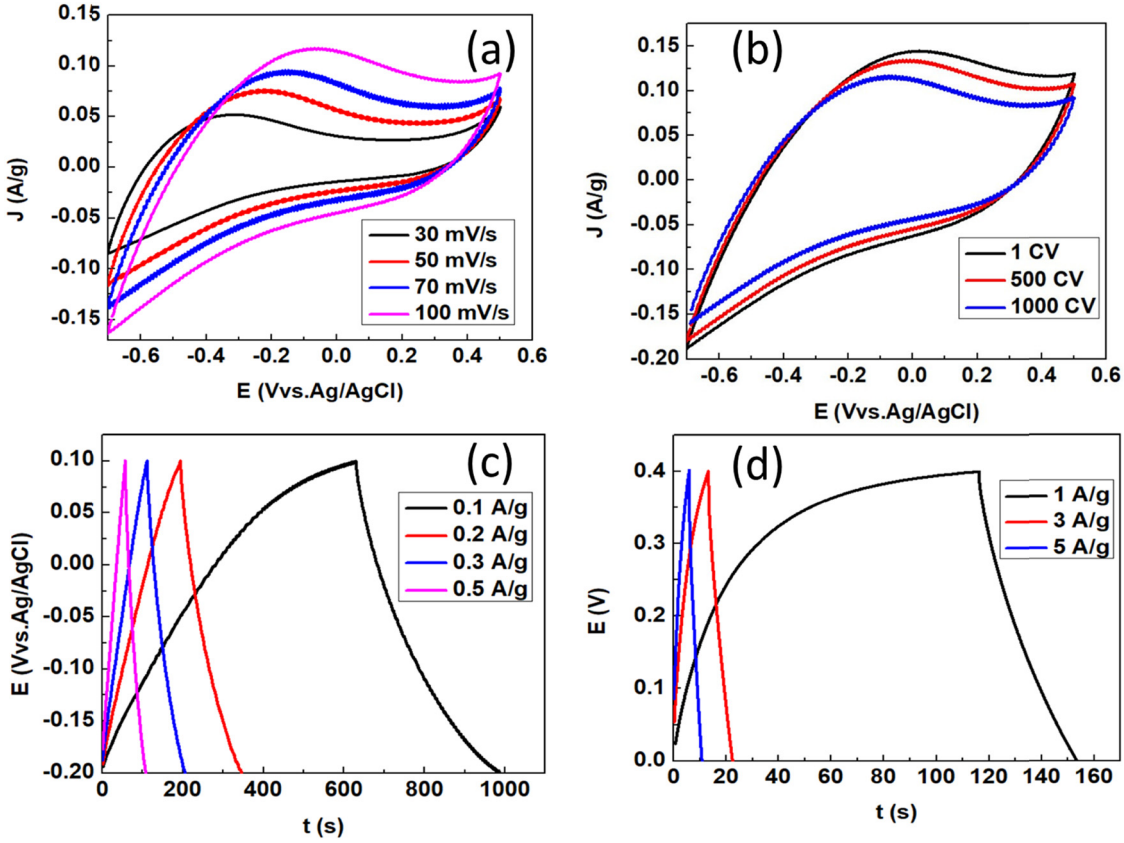

Figure 7: (a) CV spectrum of the CP electrode at 10 cycles, scanning velocity 30–100 $mV{\cdot}s^{-1}$; (b) CV spectrum of the CP electrode at 1, 500, 1,000 cycles, scanning velocity 100 $mV{\cdot}s^{-1}$; (c) discharge path depends on current density; and (d) the charge–discharge path depends on the current density of the two-electrode system.

Table 1, it can be seen that the ability of the electrode to store energy depends on the method of manufacturing the electrode material; the hydrothermal method of manufacturing CP carbon nanomaterials has better electrochemical properties for manufacturing CDPC using the improved Hummer method researched by the same group of authors [19].

In our pursuit of further research on the energy storage and release capacity of the CP electrode, we meticulously determined the energy density (E, Wh·kg^{-1}) of the CP electrode on a two-electrode system. The energy density E (Wh·kg^{-1}) of the CP electrode was calculated using a rigorous formula [12], ensuring the accuracy and reliability of our findings

$$E = \frac{1}{2}C(\Delta V)^2 \tag{3}$$

The potential scanning speed is measured at 100 mV·s^{-1}. Measuring discharge and charge with current densities of 1, 3, and 5 A·g^{-1} (Figure 6d) calculates the energy density E of the CP to be 6.4 W h·kg^{-1} corresponding to current densities of 1 A·g^{-1} and 4 W h·kg^{-1}, respectively, with a current density of 5 A·g^{-1}. Compared to the nitrogen-doped carbon material electrode (PBAC-600) with E = 7.0 W h·kg^{-1} [37], rice-straw-derived activated carbon (AA-RSC) has E = 7.8 W h·kg^{-1} [38], activated carbon material (ACN-700) has E = 6.2 W h·kg^{-1} [39], carbon nanomaterial activated by KOH combined with steam (AC-KV) made from coal [21] has E = 7.64 W h·kg^{-1}, the CP electrode has average energy density.

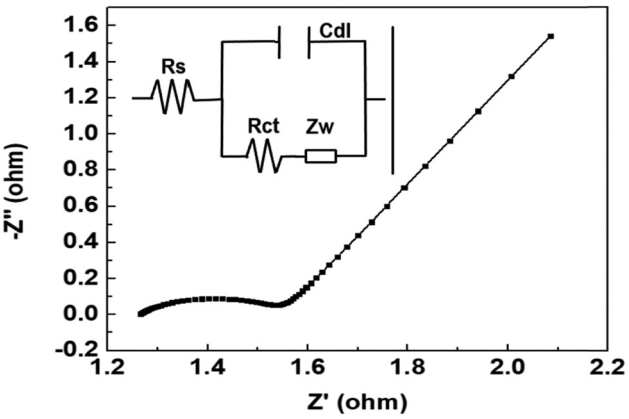

Figure 8: Nyquist spectrum of CP electrode. Inset: Equivalent circuit diagram of CP electrode [12].

3.2.3 The Nyquist spectrum

Measuring the total impedance is used to study the electrode's electrical conductivity and ion release capacity. The impedance is measured with a voltage of 0.02 V, and the frequency varies from 10 MHz to 100 kHz. The Nyquist

Table 1: Comparison of specific capacity C (F·g^{-1}) of CP with electrodes derived from coal in a 6 M KOH solution

Electrode	J (A·g^{-1})	C (F·g^{-1})	Reference
3D hollow porous graphene made from coal tar	0.05	321	[6]
Graphene capsules made of 3D from coal tar	0.05	277	[29]
Porous carbon from coal tar	2	286	[7]
Graphite from coke	0.2	192	[30]
Graphene from anthracite coal	0.05	200	[31]
Nanocarbon graphene from bituminous coal	10	230	[32]
N/S co-doped coal-based porous carbon spheres	0.2	254	[33]
Coal-based 3D hierarchical porous carbon aerogels	0.5	267	[34]
AC (Jinglong coal)	0.5	145	[12]
ACK (coal treated with KOH)	0.5	206	
ACKV (coal treated with KOH assisted with H_2O)	0.5	254	
HPCs-0.5-600-2	1.0	195	[35]
Coal-based activated carbon prepared by H_2O	1.0	194.35	[36]
Graphene quantum dots from bituminous coal	1.0	388	[8]
Nanocarbon activated by KOH combined with steam (AC-KV) from coal	0.5	254	[12]
Nanocarbon activated with KOH (AC-K) from coal	0.5	206	
Two-dimensional structured oxygen-rich porous carbon nanosheets from coal (OPCN-700)	0.5	382	[13]
Nanocarbon made by the Hummer method (CDPC)	0.1	236	[19]
	0.3	156	
Nanocarbon produced by the hydrothermal method (CP)	0.1	275	This research
	0.3	175	
	0.5	123	

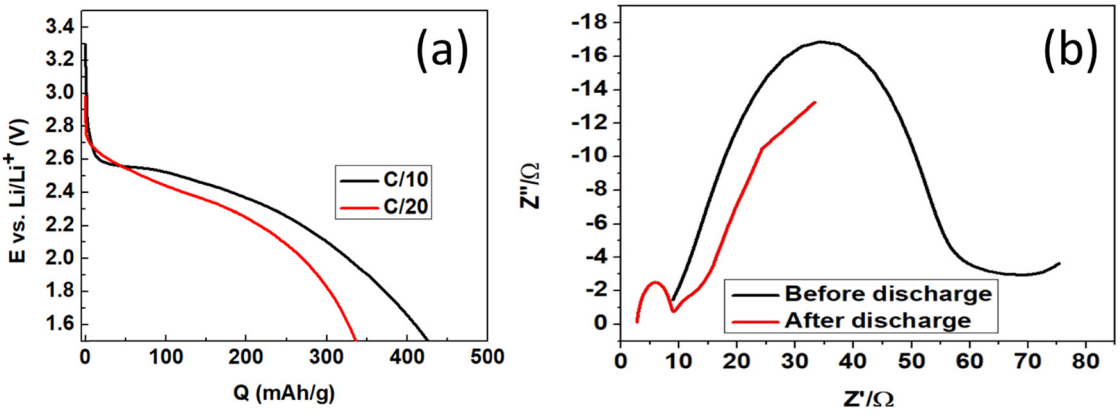

Figure 9: (a) Discharge capacity of a Li-ion battery at current density *C*/10 and *C*/20 and (b) the Nyquist spectrum before and after discharge of a Li-ion battery.

spectrum measurement results of the CP electrode are presented in Figure 8.

Figure 8a shows a straight line nearly parallel to the imaginary axis (−*Z*″), demonstrating the movement of ions in the 6 M KOH electrolyte solution. Meanwhile, the semicircle in the high-frequency region that characterizes the diffusion of CP ions is very small, demonstrating the excellent diffusion of ions within the CP structure. The diameter of the semicircle reflects the charge transfer resistance (R_{ct}). From the equivalent circuit diagram in Figure 7b [12], we can calculate R_{ct} = 0.2869 Ω. The minimal R_{ct} value shows that CP can diffuse ions well.

The electrochemical performance of the CP electrode in a 6 M KOH electrolyte solution demonstrates highly promising results for supercapacitor applications. They demonstrate that the CP material's ability to store and release energy is remarkably stable. This stability is a crucial factor in the context of energy storage, and the CP material's performance in this regard is a strong indicator of its potential as an anode electrode in LIBs.

3.3 Electrochemical measurement results of LIBs

3.3.1 Measurement of discharge by constant current

The lithium-ion storage capacity of the CP electrode was evaluated using the constant current discharge (GCD) method with current density *C*/10; *C*/20 (*C* = 372 mA h·g^{-1}), in the potential range 1.5–3.3 V (compared to Li$^+$/Li). The results of the

Table 2: Comparison of specific capacity of LIBs with anode as CP electrode and electrode derived from coal

Anode electrode material	Specific capacitance (mA h·g^{-1})	Discharge current density	Reference
Spherical porous carbon made from coal	372.0	*C*/10	[18]
Bitium coal	223.0	*C*/10	[38]
Coke	331.1	0.1 A·g^{-1}	[40]
	153.2	5 A·g^{-1}	
Graphite synthesized from anthracite coal	337.2	*C*/20	[41]
Coal treated with NaCl, Na_2CO_3	450.0	0.2 A·g^{-1}	[42]
Anthracite coal	369	0.1 A·g^{-1}	[43]
	209	1 A·g^{-1}	
Porous graphene is made from anthracite coal	770	*C*/10	[9]
CBC-700	597	1 A·g^{-1}	[44]
AC-PHC	146.4	0.1 A·g^{-1}	[35]
AC-PMC	88.8	0.1 A·g^{-1}	
HPC-3	219	10 A·g^{-1}	[45]
CP	336.0	*C*/10	This research
	425.5	*C*/20	

discharge capacity of the Li-ion battery at the current density of *C*/10 and *C*/20 of the battery are shown in Figure 9a.

From Figure 8a, the specific capacity (*Q*) of the Li-ion battery at the standard current density *C*/10 is 336.0 mA h·g^{-1} and at the current density *C*/20 is 425.5 mA h·g^{-1}.

The results of Table 2 show that the specific capacity of the Li-ion battery with an anode CP is relatively high compared to the anode electrode derived from coal. This also shows that CP as an anode in LIBs can integrate lithium ions well.

3.3.2 Total resistance measurement results

Total resistance measurements were performed with a voltage of 0.02 V, frequency varying from 10 MHz to 100 kHz. The results of measuring the Nyquist impedance of the LIB before and after discharge are presented in Figure 9b. Figure 9b shows that the Nyquist spectra before and after discharge have the exact shape of having a semicircle and a tilted line; the semicircle of the high-frequency region is related to the electric double layer capacitance and charge transfer resistance (R_{ct}), while the diffusion of Li^+ in the anode material, corresponding to the diagonal line is related to the Warburg resistance (*W*). Figure 8b shows that the battery, after discharge, has a charge transfer resistance R_{ct} (semicircle in the Nyquist spectrum) much smaller than the R_{ct} of the battery before discharge. It can be seen that after discharge, the CP anode electrode becomes more stable, and the contact between the material surface and the electrolyte solution is also better. Activated sites on the surface of CP materials also become "more active" in the interstitial Lithium-ion storage mechanism.

4 Conclusions

The CP carbon nanomaterials were fabricated using the hydrothermal method combined with $ZnCl_2$ activation. Porous carbon material CP was a two-dimensional, layered nanomaterial with a specific surface area of 16.7799 m^2·g^{-1}. CP's specific weight was 0.5 g·cm^{-3}. CP electrode worked well and stably, with the ability to maintain a capacitance of 83.1% after 1,000 CV, specific capacitance equals 275 F·g^{-1}, and energy density equals 6.4 W h·kg^{-1}. The CP electrode was assembled into an anode in a Li-ion battery. The CP electrode was capable of storing lithium ions. The specific capacity at standard current density *C*/10 was 336.0 mA h·g^{-1}, and at *C*/20, it was 425.5 mA h·g^{-1}. The $LiPF_6$ solution was in DMC, EC, and DEC at a ratio DEC/EC/DMC = 1:1:1 (v/v/v) and concentration of 1.0 M. The battery operated stably when discharged and showed a good interlocking ability of lithium ions. These results strongly indicate that CP has the potential to be a highly effective anode in LIBs, thus opening up new possibilities for energy storage technology.

Funding information: This study was supported by the ministerial-level Science and Technology project, code B2023-TNA-07, from the Viet Nam Ministry of Education and Training.

Author contributions: Tra Huong Do and Van Tu Nguyen: formal analysis; Thi Hien Lan Nguyen, Manh Chuong Chu, and Khanh Long Nguyen: data curation; Xuan Linh Ha: conceptualization; Quoc Dung Nguyen and Truong Xuan Vuong: writing-original draft preparation; Tra Huong Do, Thi Kim Ngan Tran: writing – review & editing.

Conflict of interest: Authors state no conflict of interest.

Data availability statement: The datasets generated during and/or analysed during the current study are available from the corresponding author on reasonable request.

References

[1] Wu S, Yang W, Liu Z, Li Y, Fan H, Zhang Y, et al. Organic polymer coating induced multiple heteroatom-doped carbon framework confined Co1-xS@ NPSC core-shell hexapod for advanced sodium/potassium ion batteries. J Colloid Interface Sci. 2024;660:97–105.

[2] Zhang KY, Fu YQ, Liu HH, Yang JL, Su MY, Wang Y, et al. Flaky N-doped hard carbon anode material for sodium-ion batteries. Phys Scr. 2023;98(12):125977.

[3] Qin Z. New advances in coal structure model. Int J Min Sci Technol. 2018;28(4):541–59.

[4] Mathews JP, Chaffee AL. The molecular representations of coal–A review. Fuel. 2012;96:1–14.

[5] Vasireddy S, Morreale B, Cugini A, Song C, Spivey JJ. Clean liquid fuels from direct coal liquefaction: chemistry, catalysis, technological status and challenges. Energy Env Sci. 2011;4(2):311–45.

[6] He X, Zhang H, Zhang H, Li X, Xiao N, Qiu J. Direct synthesis of 3D hollow porous graphene balls from coal tar pitch for high performance supercapacitors. J Mater Chem A Mater. 2014;2(46):19633–40.

[7] Wang H, Zhu H, Li Y, Qi D, Wang S, Shen K. Hierarchical porous carbon derived from carboxylated coal-tar pitch for electrical double-layer capacitors. RSC Adv. 2019;9(50):29131–40.

[8] Qing Y, Jiang Y, Lin H, Wang L, Liu A, Cao Y, et al. Boosting the supercapacitor performance of activated carbon by constructing overall conductive networks using graphene quantum dots. J Mater Chem A Mater. 2019;7(11):6021–7.

[9] Xing B, Zeng H, Huang G, Zhang C, Yuan R, Cao Y, et al. Porous graphene prepared from anthracite as high performance anode materials for lithium-ion battery applications. J Alloy Compd. 2019;779:202–11.

[10] Le MK, Tran TN, Huynh TKT, Vo DT, Le MLP. Development of Vang Danh anthracite as a cost-effective anode for sodium-ion batteries through a heat-treatment process. RSC Adv. 2022;12(46):29900–7.
[11] Li J, Cao YL, Wang LX. Performance of coal-derived spherical porous carbon as anode materials for lithium ion batteries. J Inorg Mater. 2017;32(9):909–15.
[12] Dong D, Zhang Y, Wang T, Wang J, Romero CE, Pan WP. Enhancing the pore wettability of coal-based porous carbon as electrode materials for high performance supercapacitors. Mater Chem Phys. 2020;252:123381.
[13] Che XG, Jin J, Zhang YX, Liu SY, Wang M, Yang J. Fabrication of coal-based oxygen-rich porous carbon nanosheets for high-performance supercapacitors. N Carbon Mater. 2023;38(6):1050–8.
[14] Yang N, Ji L, Fu H, Shen Y, Wang M, Liu J, et al. Hierarchical porous carbon derived from coal-based carbon foam for high-performance supercapacitors. Chin Chem Lett. 2022;33(8):3961–7.
[15] Qie Z, Wang L, Sun F, Xiang H, Wang H, Gao J, et al. Tuning porosity of coal-derived activated carbons for CO2 adsorption. Front Chem Sci Eng. 2022;16(9):1345–54.
[16] Yin Y, Liang D, Liu D, Liu Q. Preparation and characterization of three-dimensional hierarchical porous carbon from low-rank coal by hydrothermal carbonization for efficient iodine removal. RSC Adv. 2022;12(5):3062–72.
[17] Han G, Jia J, Liu Q, Huang G, Xing B, Zhang C, et al. Template-activated bifunctional soluble salt ZnCl2 assisted synthesis of coal-based hierarchical porous carbon for high-performance supercapacitors. Carbon N Y. 2022;186:380–90.
[18] Dopita M, Rudolph M, Salomon A, Emmel M, Aneziris CG, Rafaja D. Simulations of X-Ray Scattering on Two-Dimensional, Graphitic and Turbostratic Carbon Structures. Adv Eng Mater. 2013;15(12):1280–91.
[19] Do TH, Nguyen VT, Nguyen TN, Ha XL, Nguyen QD, Tran TKN. Synthesis of porous carbon nanomaterials from Vietnamese coal: fabrication and energy storage investigations. Appl Sci. 2024;14(3):965.
[20] Bonhomme F, Lassegues JC, Servant L. Raman spectroelectrochemistry of a carbon supercapacitor. J Electrochem Soc. 2001;148(11):E450.
[21] Fromm O, Heckmann A, Rodehorst UC, Frerichs J, Becker D, Winter M, et al. Carbons from biomass precursors as anode materials for lithium ion batteries: New insights into carbonization and graphitization behavior and into their correlation to electrochemical performance. Carbon N Y. 2018;128:147–63.
[22] Lee SE, Kim JH, Lee YS, Bai BC, Im JS. Effect of crystallinity and particle size on coke-based anode for lithium ion batteries. Carbon Lett. 2021;31:911–20.
[23] Jawad AH, Nawi MA, Mohamed MH, Wilson LD. Oxidation of chitosan in solution by photocatalysis and product characterization. J Polym Env. 2017;25:828–35.
[24] Coates J. Interpretation of infrared spectra, a practical approach. Encycl Anal Chem. 2000;12:10815–37.
[25] Zhang Z, Xu L, Liu Y, Feng R, Zou T, Zhang Y, et al. Efficient removal of methylene blue using the mesoporous activated carbon obtained from mangosteen peel wastes: Kinetic, equilibrium, and thermodynamic studies. Microporous Mesoporous Mater. 2021;315:110904.
[26] Gregg SJ, Sing KSW, Salzberg HW. Adsorption surface area and porosity. J Electrochem Soc. 1967;114(11):279Ca.
[27] Sing KSW, Williams RT. Physisorption hysteresis loops and the characterization of nanoporous materials. Adsorpt Sci Technol. 2004;22(10):773–82.
[28] Sing KSW. Reporting physisorption data for gas/solid systems with special reference to the determination of surface area and porosity (Recommendations 1984). Pure Appl Chem. 1985;57(4):603–19.
[29] He X, Li X, Ma H, Han J, Zhang H, Yu C, et al. ZnO template strategy for the synthesis of 3D interconnected graphene nanocapsules from coal tar pitch as supercapacitor electrode materials. J Power Sources. 2017;340:183–91.
[30] Thomas R, Balachandran M. Luminescence and energy storage characteristics of coke-based graphite oxide. Mater Chem Phys. 2021;257:123854.
[31] Kim JP, Choi HK, Chang YJ, Jeon CH. Feasibility of using ash-free coal in a solid-oxide-electrolyte direct carbon fuel cell. Int J Hydrog Energy. 2012;37(15):11401–8.
[32] Zhang S, Zhu J, Qing Y, Fan C, Wang L, Huang Y, et al. Construction of hierarchical porous carbon nanosheets from template-assisted assembly of coal-based graphene quantum dots for high performance supercapacitor electrodes. Mater Today Energy. 2017;6:36–45.
[33] Lv Y, Chen J, Jia W, Wu X, Guo J, Ding L, et al. N/S co-doped coal-based porous carbon spheres as electrode materials for high performance supercapacitors. RSC Adv. 2020;10(19):11033–8.
[34] Lv Y, Ding L, Wu X, Guo N, Guo J, Hou S, et al. Coal-based 3D hierarchical porous carbon aerogels for high performance and super-long life supercapacitors. Sci Rep. 2020;10(1):7022.
[35] Ferdous AR, Shah SS, Shah SNA, Johan BA, Al Bari MA, Aziz MA. Transforming waste into wealth: Advanced carbon-based electrodes derived from refinery and coal by-products for next-generation energy storage. Molecules. 2024;29(9):2081.
[36] Xiong S, Lv F, Wang C, Yang N, Zhang Y, Duan Q, et al. Coal-based activated carbon prepared by H_2O activation process for supercapacitors using response surface optimization method. Front Chem Sci Eng. 2024;18(6):63.
[37] Niu L, Shen C, Yan L, Zhang J, Lin Y, Gong Y, et al. Waste bones derived nitrogen–doped carbon with high micropore ratio towards supercapacitor applications. J Colloid Interface Sci. 2019;547:92–101.
[38] Sudhan N, Subramani K, Karnan M, Ilayaraja N, Sathish M. Biomass-derived activated porous carbon from rice straw for a high-energy symmetric supercapacitor in aqueous and non-aqueous electrolytes. Energy Fuels. 2017;31(1):977–85.
[39] Shen C, Li R, Yan L, Shi Y, Guo H, Zhang J, et al. Rational design of activated carbon nitride materials for symmetric supercapacitor applications. Appl Surf Sci. 2018;455:841–8.
[40] Liu Y, Guo X, Tian X, Liu Z. Coal-based semicoke-derived carbon anode materials with tunable microcrystalline structure for fast lithium-ion storage. Nanomaterials. 2022 Nov;12(22):4067.
[41] Wang T, Wang Y, Cheng G, Ma C, Liu X, Wang J, et al. Catalytic graphitization of anthracite as an anode for lithium-ion batteries. Energy Fuels. 2020 Jul;34(7):8911–8.
[42] Gao S, Tang Y, Wang L, Liu L, Sun Z, Wang S, et al. Coal-based hierarchical porous carbon synthesized with a soluble salt self-assembly-assisted method for high performance supercapacitors and li-ion batteries. ACS Sustain Chem Eng. 2018 Mar;6(3):3255–63.
[43] Li Y, Tian XD, Song Y, Yang T, Wu SJ, Liu ZJ. Preparation and lithium storage of anthracite-based graphite anode materials. N Carbon Mater. 2022;37(6):1163–9.
[44] Chen Z, Zhang A, Geng C, Xiong J, Sun P, Tu N, et al. Coal-based hierarchical porous carbon for lithium/potassium storage. Mater Chem Phys. 2023;303:127835.
[45] Zhang M, Qu M, Yuan W, Mu J, He Z, Wu M. Green synthesis of hierarchically porous carbon derived from coal tar pitch for enhanced lithium storage. Batteries. 2023;9(9):473.